Colloids and Surfaces B: Biointerfaces 171 (2018) 383–390

Contents lists available at ScienceDirect

Colloids and Surfaces B: Biointerfaces

journal homepage: www.elsevier.com/locate/colsurfb

Biological and optical properties of sol–gel derived ZnO using different percentages of silver contents

Zohra Nazir Kayani[a,*], Maryam Anwar[a], Zeb Saddiqe[a], Saira Riaz[b], Shahzad Naseem[b]

[a] Lahore College for Women University, Lahore, 54000, Pakistan
[b] Centre of Excellence in Solid State Physics, University of the Punjab, Lahore, 54950, Pakistan

ARTICLE INFO

Keywords:
Sol–gel
Structural properties
Optical band gap
Ag doped ZnO
Antibacterial study

ABSTRACT

The role of Ag dopant on ZnO thin films are studied. Ag doped ZnO thin films were deposited by sol–gel dip coating on glass substrates. The X-ray diffraction analysis shows hexagonal wurtzite with preferred orientation along the (101) plane. The crystallite size decreases from 33.40 nm to 28.37 nm with increase in silver doping percentage. Optical examination shows that the band gap decrease with an increase in the Ag doping in ZnO. The structural and optical results prove that Ag has substituted Zn in ZnO lattice. Silver doped ZnO is effective against *Staphylococcus aureus (S. aureus)* and *Pseudomonas aeruginosa (P. aeruginosa)* bacteria. The roughness and the surface oxygen species accelerate the bacteria killing properties of Ag doped ZnO. They have pharmacological utility as a replacement of the antibiotics, bactericide and disinfectants. The TGA study showed that the thermal stability of the Ag doped ZnO takes place between 380–435 °C.

1. Introduction

Zinc oxide (ZnO) is an inexpensiveand the most used materials for integration in dilute magnetic semiconductors and biotechnology. Originally it is of 3.37 eV wide band gap material and have 60 meV exciton binding energy. These properties are beneficial in number of photonic applications [1]. Due to it's piezoelectricity, it finds applications in window materials for display, solar cells [2], gas-bio sensors [3,4] and actuators [5]. It acts as a bactericide [6], photocatalyst [7], infection prevention [8,9] and biomedical implants [10].

A lot of research is conducted to tailor the properties of ZnO by using doping [11–13]. The characteristics of ZnO thin films are also dependent on the deposition specifications and different deposition routes. Metal ion doping [14,15] with the ZnO is taken as the best approach to improve the electrical, semi-conducting, magnetic, antibacterial, photo-catalytic, thermal and optical properties. Among metal, silver is considered as the best choice owing to its high solubility, small orbital energy and large ionic size [16]. Silver has been used to kill bacteria [17,18] and Ag/ZnO is used to accelerate healing wound [19]. Silver ions have two distinct characteristics. It can take interstitial position in ZnO or can substitute Zn^{2+} ions in ZnO and; so, they can act as an acceptor in ZnO. It is difficult to obtain absorption of visible light on undoped ZnO. Ag doped ZnO is a promising choice being wide band gap material to absorb light without showing and toxicity. It finds applications in window of solar cell [20]. Ag-doped ZnO is highly sensitive and responsive than ZnO. So Ag doped ZnO enhances the electrochemical properties and the sensing abilities. Thus, Ag doped ZnO nano-materials are ideal sensors for the number of toxic and harmful gases [15]. Ag is a competible material with ZnO to improve photocatalytic properties of ZnO [21]. Silver ions impinge on the surface of ZnO creates a new energy level that can capture the photogenerated electrons from the conduction band of ZnO, and so reduces the electron hole pair (EHP) recombination [22]. Ag doped ZnO not only enhance the photocatalytic properties, but the creation of reactive species improves the bacterial killing rate. Ag doped ZnO possesses an antibacterial property which is useful to treat waste water [23], curative -preventive health care and other environmental applications [24]. Ag/ZnO composites are used in biomedical application in orthopedic, dental implants and infection prevention [25,26].

To explore the thin films of Ag doped ZnO, several methods such as magnetron sputtering [27], sol–gel spray coating [28], spin coating [20,29] and chemical vapour deposition [30] were used to deposit thin films. However, there are few studies on the synthesis of Ag doped ZnO thin films on the glass substrate by sol–gel dip coating technique. This technique is cost-effective, straight forward and can be conducted at room or low temperature. That's why, in this paper, the simple sol–gel dip coating technique was used to deposit Ag: ZnO thin films on the glass substrate with various doping concentrations of Ag. Role of Ag

* Corresponding author.
E-mail address: zohrakayani@yahoo.com (Z.N. Kayani).

https://doi.org/10.1016/j.colsurfb.2018.07.055
Received 21 May 2018; Received in revised form 19 July 2018; Accepted 24 July 2018
Available online 25 July 2018
0927-7765/

doping on the optical, magnetic, antibacterial and structural properties of ZnO thin films were explored. Their antibacterial activity was conducted to monitor inhibition of the growth of *Pseudomonas aeruginosa (P.A)* the Gram-negative bacteria and *Staphylococcus aureus (SA)* the Gram-positive bacteria. *S. aureus* is usually found in the respiratory tract, the nose and on the skin while *P. Aeruginosa* can be found in any part of the body. Generally the Gram-negative bacteria are difficult to destroy than Gram-positive bacteria because the wall of the cell Gram-negative bacteria have an outer membrane that protects the peptidoglycan layer [31]. It is also helpful for the survival of bacteria by shielding them from any external harm.

2. Experimental

The methodology for deposition of Ag doped ZnO thin films was started with the preparation of sol. Firstly, a 0.05 M solution of zinc acetate dehydrate ($Zn(CH_3COO)_2.2H_2O$, Aldrich, 99.9%) was dissolved in isopropanal under magnetic stirring. For Ag doping, the silver nitrate (AgNO3, Aldrich, 99.8%) was chosen as a doping source. In similar 0.05 M sol of $Ag(NO_3)_3$ was prepared. Afterwards, both sols of Zn and Ag were mixed and stirred. After stirring the sol for about 30 min, few drops of diethyl amine were added and the sol was stirred for three hours at room temperature. In this way five sols were prepared by varying Ag dopant percentage between 02–10 wt.at%. The films were dip coated on glass substrates which were ultrasonically pre-cleaned. The Ag-doped ZnO thin films with different percentages of silver dopant were then deposited on glass substrates by dipping them in sols and then withdrawing at a constant withdrawal speed of 250 mm/sec. After the dip coating process, the films were dried at 150 °C for 10 min to evaporate the solvents and organic residuals. This process was repeated 5 times to achieve optimized thickness. Afterwards, all the thin films were annealed at 500 °C for 4 h in air.

The Fourier transform infrared (FTIR) transmittance measurements were done by FTIR Model M 2000 Midac USA spectrophotometer in the spectral range from 400 cm^{-1} to 3000 cm^{-1}. Ag doped ZnO was studied by thermo gravimetric analysis and differential scanning calorimetry (TGA/DSC) using a SDT Q600 instrument to record the effect of the thermal behaviour of the Ag doped ZnO. The TGA/DSC responses were conducted at a constant heating rate of 2 K/min in the air. The surface morphology was studied by field emission SEM using a Zeiss Evo Ls 10 Germany. The structure of the thin films was analysed by XRD (D 8 Discover, Bruker Germany). θ–2θ spectra were recorded between 2θ = 20°–80° in 0.04° steps with time/step 0.5 s. Tube current was 40 mA and tube voltage 40 KV. Optical Transmission was conducted in the wavelength range of 300–900 nm by using (Hitachi 2800 U) UV–vis spectrophotometer.

3. Results and discussions

3.1. FTIR

Ag doped ZnO thin films were analysed by FTIR in the range from 450 to 4000 cm^{-1} as shown in Fig. 1. The FT-IR spectra of the Ag doped ZnO thin films have many absorption bands. The bands between 400–650 cm^{-1} are due to Zn−O band [32]. Bands around 750–900 cm^{-1} are due to the stretching and bending frequency of Ag and ZnO [14]. A band observed in the region ~ 1120 cm^{-1} is due to C−O−C coupling [32]. Bands at 1383 cm^{-1} and 1506 cm^{-1} corresponds to C−O and C═O bending vibrations respectively [32]. The weak but wide band near 1636 cm^{-1} is assigned to the O−H−O bending vibration mode [33]. The O═C═O dip is located at around 2341.21cm^{-1}. The band at 3439.49 cm^{-1} displays the presence of OH group [32]. According to Fig. 1, a slight shift in frequency with increasing silver, Ag doping can be seen. This shift in the absorption band toward lower frequencies might be due to the changes in bond length after substitution of Ag^{3+} ion in the ZnO lattice. The FTIR data confirmed Ag successful doping in ZnO.

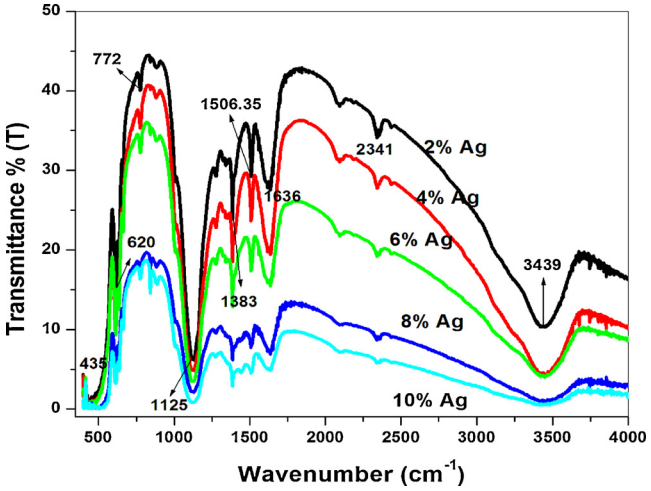

Fig. 1. FTIR spectra of Ag doped ZnO thin films.

3.2. TGA/DSC

To study the crystalline conditions, differential scanning colorimetry (DSC) and TGA of Ag doped ZnO were conducted. The materials were heated from room temperature to 1100 °C with an increment of 10 °C/min in the air. Fig. 1 shows plots of DSC and TGA. Ag remained stable in ZnO and thermally decomposed to Ag ion between 200–270 °C [34]. The thermo-gravimetric analysis (TGA) plots of Fig. 2 revealed the weight loss in two main temperature ranges, (70 °C–200 °C) and (295 °C–370 °C). The weight loss around the temperature range (70 °C–200 °C) was due to the loss of water and isopropanol. The weight loss in the temperature range (290 °C–370 °C) was due to the loss of acetate and nitrate groups [35]. In the TGA plot the weight loss took place till 370 °C. It is seen that the 10 wt. % Ag doped ZnO has the most residual weight, thus it can be said to be more thermally stable than the other doping percentages. For the DSC curve, two endothermic peaks and an exothermic peak are found at 242–255, 330–350, 386–420 °C, respectively for different Ag doping wt.%. These endothermic peaks are due to the evaporation of water and organics. A large exothermic peak was due to the crystallization of ZnO. Hence, the crystallization of Ag doped ZnO took place round about 500 °C. For this reason, films of Ag doped ZnO were annealed at 500 °C for crystallization.

3.3. Surface morphology

Fig. 3 presents the SEM micrographs of Ag doped ZnO thin films. Fig. 3(a) and (b) show thin flakes [36] with voids or holes with highly agglomerated grain on thin film. Generally, if the Ag is not incorporated into the ZnO lattice [37], it is detached at the grain boundary. The detached Ag gathers at the grain boundary and hinder the grain growth. This crack-free morphology is essential for the antibacterial material to protect against the presence of bacterial colonies. Fig. 3(c) and (d) show that with the increase in the Ag doping percentage to 10 wt% film is not continuous but patchy showing dendrite features. Grains are inclined to form clusters and show irregular dendrite structure. This morphology is important for photocatalytic applications.

3.4. Structural properties

Fig. 1 displays the XRD patterns of Ag doped ZnO thin films, which show that all thinfilms have hexagonal structure. The X-Ray diffraction pattern showed polycrystalline thin films with a preferred orientation of (101). All diffraction peaks (100), (002), (101), (102), (110), (103),

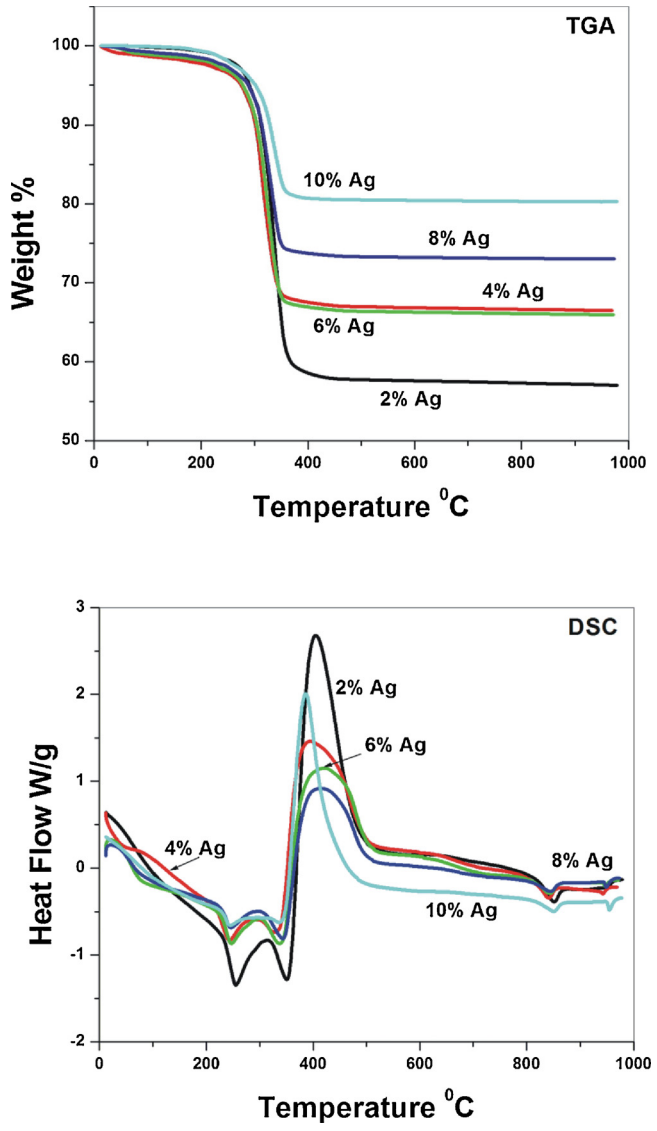

Fig. 2. TGA and DSC of Ag doped ZnO with 2–10 wt.% Ag.

(200), (112), (201) and (004) are matched with ZnO by the Joint Committee on Powder Diffraction Standards (JCPDS) card for ZnO (JCPDS036-1451). Four XRD peaks of (111), (200), (220) and (311) planes are due to the metallic silver fcc phase (JCPDS04-0783) confirm Ag as the secondary phase clusters and with increase in Ag dopant percentage, the intensity of these peaks varied. Ag ions are incorporated into the ZnO lattice at either the interstitial positions or substitute Zn in ZnO lattice. Thin films display impurity peaks of to Ag or Ag dioxides, predicting that the solubility of Ag in ZnO is low. Ag or Ag dioxides are formed due to the generation of silver clusters in the sol and these Ag clusters precipitate or not adsorbed on the glass substrate in the process of dip coating. Secondly Ag ions have ability to reduce to metallic silver. Thirdly, the momentum of hydrolysis and condensation undermine the hydrolyzed complexes of Ag in the sol and promote the generation of Ag or silver oxide such as Ag_2O or AgO. The X-ray diffraction pattern for Ag-doped ZnO thin films confirmed that the thin films are free of any detectable impurity (Fig. 4).

The intensities of all the peaks are decreased for Ag doping between 2–6%. Further increase in doping resulted in an increase in the (101) peak intensity which again decreased at 10% Ag doping. It points out that the crystallinity initially decreased Ag doping. The peak due to the (101) plane is the most intense peak. After incorporation of 2–6% Ag, the peak position of the (101) plane was slightly shifted toward the lower 2θ value. For further increases of Ag content, the preferred oriented peak shifted toward the higher 2θ values but remain along (101) plane.

The crystallite size was calculated from the Scherrer formula [38]:

$$D = k\lambda/\beta\cos\theta$$

Where β is FWHM; θ is Bragg angle, λ is 1:54 Å (X-ray wavelength) and k is 0:9. By applying the Debye–Scherrer equation, the average crystallite size was found to be in the range 35.4–28.34 nm from the FWHM of the dominant peak (101). The changes in the crystallite size revealed that the crystalline behaviour of nanocomposite film decreased. The crystallinity of the films is affected by the Ag dopant percentage which are linked to the lattice strain between the crystallite of the Ag doped ZnO thin films. As Ag is less soluble in ZnO, so Ag atoms are absorbed in the grain boundaries or on the film surface reducing the crystallite size. It can be concluded that the percentage of Ag can influence the crystallite size of ZnO. Decrease in crystallite size is also observed by other researchers [39,40].

The dislocation density δ, is the length of dislocation lines per unit volume, which is evaluated by using the equation [39]:

$$\delta = 1/D^2$$

Stress and strain is generated during deposition due to the lattice mismatch between Ag doped ZnO thin film and glass substrate. So, the stress and strain modify the structural properties of Ag doped ZnO thin films. The strain can be calculated by the following formula

$$\varepsilon = \beta\cos\theta/4$$

where ε is the mean strain in ZnO thin films and stress can be calculated by the relation

Number of crystallites per unit area (N) are calculated by applying formula

$$N = t/D^3$$

Wher t is thickness of films and D is the crystallite size.

The dislocation density δ, strain ε and number of crystallites N show increasing trend with increase in Ag dopant percentage which show increase in lattice imperfection.

The lattice constants for the Ag doped ZnO thin films on glass substrates were evaluated from the following relations. The lattice constant 'a' was assessed by

$$a = \lambda/(3)^{1/2}\sin\theta_{100}$$

The lattice constant 'c' was calculated by the equation

$$c = \lambda/\sin\theta_{002}$$

The lattice constant "a" minutely increases with the Ag doping whereas "c" increases more significantly, which increase the volume of the cell (Table 1b). Lattice constant "a" and "c" for un-doped ZnO are 3.249 Å and 5.206 Å respectively while volume of unit cell is 47.62Å^3. The larger radius of Ag^+ ions (0.126 nm) compared to Zn^{2+} ions (0.074 nm) is responsible for this increase. Difference in the ionic radius of Ag^+ ion and Zn^{+2} is responsible possible for some Ag^+ ion to substitute for Zn^{2+} ion and few Ag^+ aggregate in an Ag cluster. It is assumed that when the Ag dopant percentage in solution is ≥2 wt. %, then the Ag constitutes a cluster as well as substitutes the Zn^{2+} in the ZnO lattice. The Ag clusters in are also confirmed in ZnO thin films by the XRD analysis. It means that Ag does not completely incorporated into the ZnO lattice, it detaches at the grain boundary. The detached Ag clusters at the grain boundary then act as an obstacle that halts the grain growth. For 10% Ag-doped ZnO samples, "a" and "c" decreases, which is due to nano-clusters. Formation of nano-clusters are also confirmed by SEM.

All structural properties are provided in Tables 1a and 1b. Table 1a shows crystallite size, strain, dislocation density, Number of crystallite and lattice constants while Table 1b shows X-Ray density, volume of

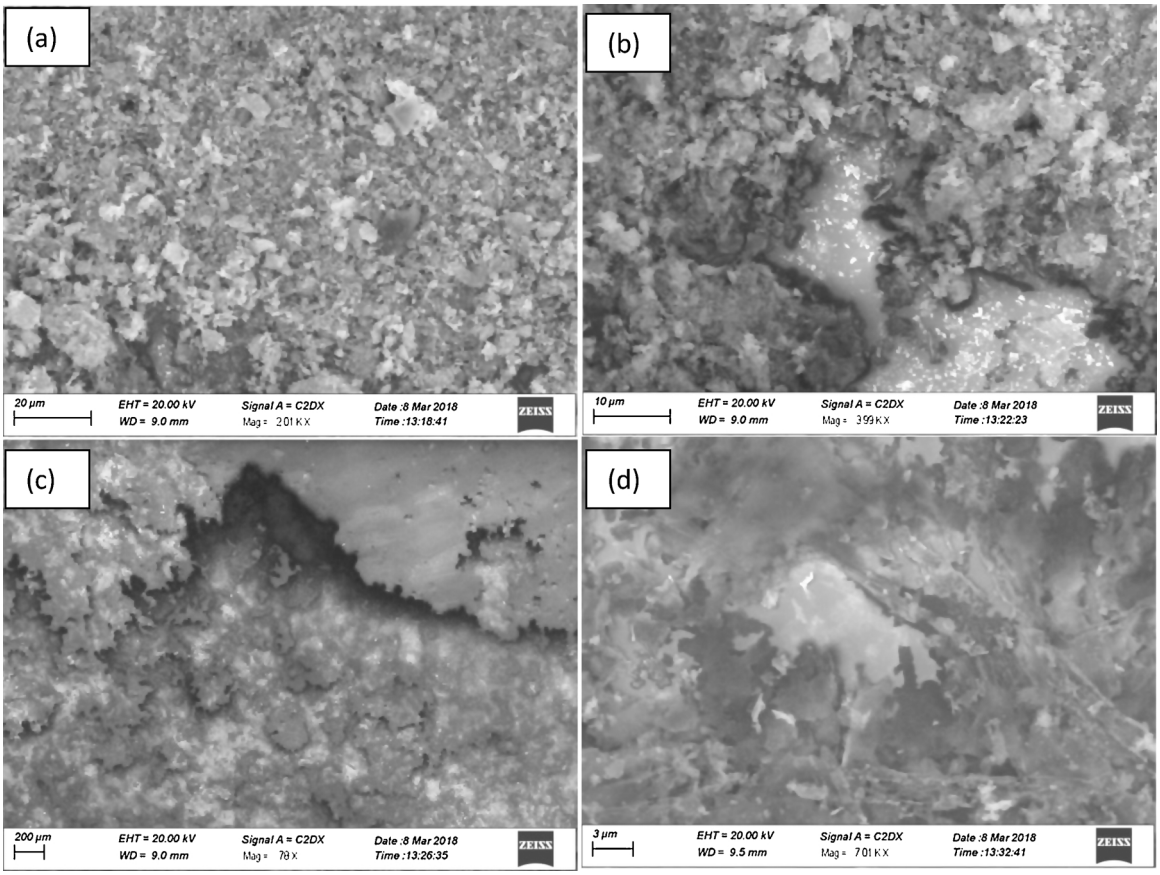

Fig. 3. SEM images of Ag doped ZnO thin films deposited with (a) 4 wt % Ag at low magnification (b) 4 wt % Ag at high magnification, (c) 10 wt % Ag at low magnification and (d) 10 wt% Ag at high magnification.

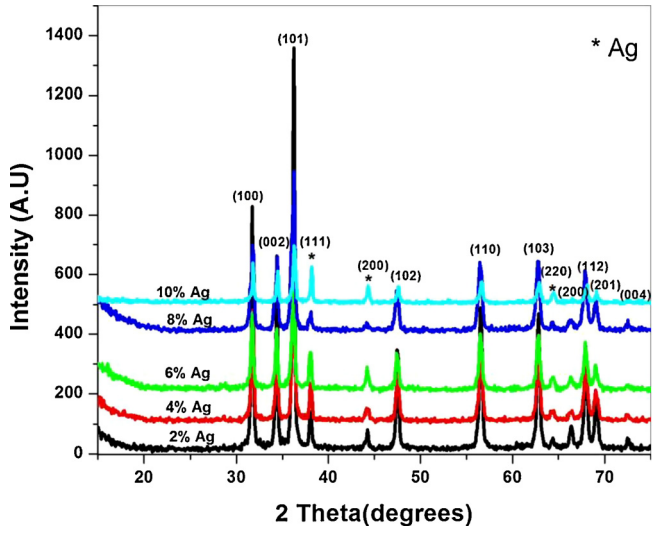

Fig. 4. XRD spectra of Ag doped ZnO thin films with Ag dopant.2–10%.

unit cell, energy density, bond length and stress.

Volume of unit cell and X-Ray density are calculated by relations

$$\text{Volume} = V = 0.866a^2c$$

$$X - Raydensity = 8M/N_a a^3$$

The volume of unit cell and X-Ray density of films is modifying with changes in lattice constants.

The bond length L is evaluated by the relation [33]

$$L = \sqrt{a^2/3 - (1/2 - u)^2 c^2}$$

where u is defined as

$$u = a^2/2c^2 + 0.25$$

Table 1b shows that the bond length of Ag doped ZnO thin films is less than bond length of undoped ZnO 1.9767 Å.

For hexagonal crystals stress (σ) is calculated by relation

$$\sigma = \varepsilon Y_{hkl}$$

Total stress is due to intrinsic defects, dislocations and oxygen vacancies while extrinsic stress is produced due to lattice mismatching of film and substrate.

Where Y is Young'Modulus whose value is calculated by

$$Y_{hkl} = [h^2 + (h + 2K)^2/3 + (al/c)^2]/S_{11}(h^2 + (h + 2K)^2/3)^2 + S_{33}(al/c)^4 + (2S_{13} + S_{44})(h2 + (h + 2K)^2/3)(al/c)^2$$

where S_{11}, S_{13}, S_{33}, S_{44} are the elastic compliances of ZnO with values of 7.858×10^{-12}, -2.206×10^{-12}, 6.940×10^{-12}, $23.57 \times 10^{-12}\ m^2\ N^{-1}$

Energy density u (energy per unit volume) can be evaluated by

$$u = \varepsilon^2 Y_{hkl}/2$$

Where Y is Young'Modulus and ε is the strain. Energy density is varying with increase in Ag dopant percentage.

3.5. Optical properties

The optical parameters of the Ag doped ZnO thin films were recorded by the transmission curves plotted between wavelength of 300–900 nm. 2% Ag-doped ZnO has a transparency of around 55–65%

Table 1a
Primary structural properties of Ag-doped ZnO thin films.

Doping (%)	Crystallite size, D (nm)	Dislocation density,δ (n/m^2) (10^{-4})	Strain, ε (10^{-4})	Number of crystallites/m^3 (10^{-5})	lattice constant		
					'a'	'c'	c/a
2%	35.40	7.978	12.22	8.052	3.255	5.212	1.601
4%	35.396	7.981	10.19	8.095	3.249	5.206	1.602
6%	35.393	7.982	9.79	9.214	3.256	5.217	1.602
8%	33.995	8.653	9.787	9.595	3.249	5.206	1.602
10%	28.37	12.428	9.787	11.359	3.246	5.201	1.602

Table 1b
Secondary structural properties of Ag-doped ZnO thin films.

Doping (%)	Vol of unit cell (V) (Å^3)	X-ray density g/molÅ^3 (10^{-23})	Stress,(σ) (Mpa) (10^8)	Energy density u (KJm^{-3}) (10^4)	Bond Length (L) (Å)
2%	47.8199	8.4549	1.1635	5.6955	1.8738
4%	47.5895	8.5034	1.1631	5.6920	1.8539
6%	47.9686	8.4285	1.4518	8.8673	1.8386
8%	47.5895	8.5034	1.1631	5.6920	1.8539
10%	47.4620	8.5246	1.211	6.1728	1.8522

in the visible region and the fringes come into view. The high transparent film is deposited by the substitution of 2% Ag atoms in place of Zn atoms which provide space between particles and allow light to easily pass. This is also supported by SEM micrographs. Further increase in Ag dopant percentage decrease transmission. This decreased transmission is the result of the reduction of metal crystallite size. Increase in dopant percentage move absorption edge toward the visible light wavelength. Increase in scattering in thin films is due to increase in roughness and oxygen vacancies of thin films with an increase in the Ag dopant percentage which decrease the optical transmission. These films can be used as photocatalyst and transparent window materials in many optoelectronic devices.

The T (transmission) values were used to evaluate the values of the band gap (Eg) of the Ag doped ZnO thin films. The band gap was calculated according the Tauc model. The absorption coefficient (α) and photon energy for direct transitions are related by equation [41]

$$\alpha h\nu = (h\nu - E_g)^{1/2}$$

Where hν is the photon energy, α is the absorption coefficient, A is a constant dependent on the mobility of electron-hole and Eg is the optical band gap energy.

The intersections on the energy axis provide the band gap (Eg) values by extrapolation of the straight-line section of the $(\alpha h\nu)^2$ versus hν curve, The Eg values recorded are (3.19, 3.16, 3.13, 3.12 and 3.10) eV. The band gap of all the thin films is lower than that of the pure ZnO (3.3 eV) [42]. This decrease in the band gap with an increase in Ag dopant percentage is also observed by Xian et al. [20], Feroz et al. [14]. and Hosseini [43]. This red shift in band gap can be explained on the basis of impurity bands. Silver doping in ZnO imparts the impurity band in the energy band gap due to overlapping of Ag and O states. This reduction proves that silver dopant is substituted into the zinc sites which imparts an energy acceptor level in the band gap. This reduction in band gap energy is beneficial in the optoelectronic devices [44].

The calculated refractive index of the deposited thin films increases with increase in Ag dopant concentration. The values of n vary between 1.55–1.59. The band gap for the samples decreases with increase in refractive index [45,46].

The extinction coefficient (K) deals with the exponential decay of the electro Magnetic wave in the thin films. The extinction coefficient is defined by the formula [47]

$$k = \alpha\lambda/4\pi$$

The extinction coefficient shows the dispersion trend obeying the Sellmeier relationship of extinction coefficient. Extinction coefficient decreases with increase in Ag doping percentage. Stronger absorbing medium shows the higher extinction coefficient

The amplitude of electromagnetic wave is decreased by a factor 'e' after covering a thickness of film is the skin depth χ [48] such that:

$$\chi = \lambda / 2\pi k_0$$

Table 2 shows the variation of skin depth as a function of wavelength for ZnO with different Ag dopant percentage. Table 2 shows that skin depth decreases with increase in Ag dopant percentage.

The optical conductivity is represented by [49]

$$\sigma = \alpha nc/4\pi$$

The optical conductivity enhances with an increase in Ag dopant percentge due to the addition of charge carriers. Change of extinction coefficient, optical conductivity and skin depth are shown in Table 2.

The absorption coefficient in the energy region of $h\nu < Eg$, is govern by Urbach formula [50]:

$$\alpha = \alpha_0 \exp\left(\frac{h\nu}{E_U}\right)$$

where E_U is Urbach energy and α_0 are constants. The above quation depicits the optical transition between the valence band tail to the conduction band edge. The structure disorder is due to defects and doping which emerge Urbach tail. A plot of ln α versus hν should be linear and Urbach energy is evaluated from the slope. The evaluated values of optical properties are listed in Table 2. The E_U increases and Eg decreases with increase in Ag dopant percentage. The increase of E_U predicts that the atomic structural disorder of films increase and which is also cause of the decrease of optical transmission.

Table 2
Optical Properties of Ag doped ZnO thin films.

Ag doping %	Thickness μm	Band Gap Eg (ev)	Skin Depth χ	Extinction coefficient k	Optical conductivity (σ)	Refractive Index n	Urbach Energy (ev)
2%	2.19	3.19	0.105	0.014	0.015	1.54	0.06
4%	3.57	3.16	0.100	0.0098	0.030	1.55	0.07
6%	3.59	3.13	0.093	0.0073	0.041	1.56	0.2
8%	3.62	3.12	0.067	0.0069	0.048	1.57	0.15
10%	5.04	3.1	0.047	0.0063	0.091	1.59	0.17

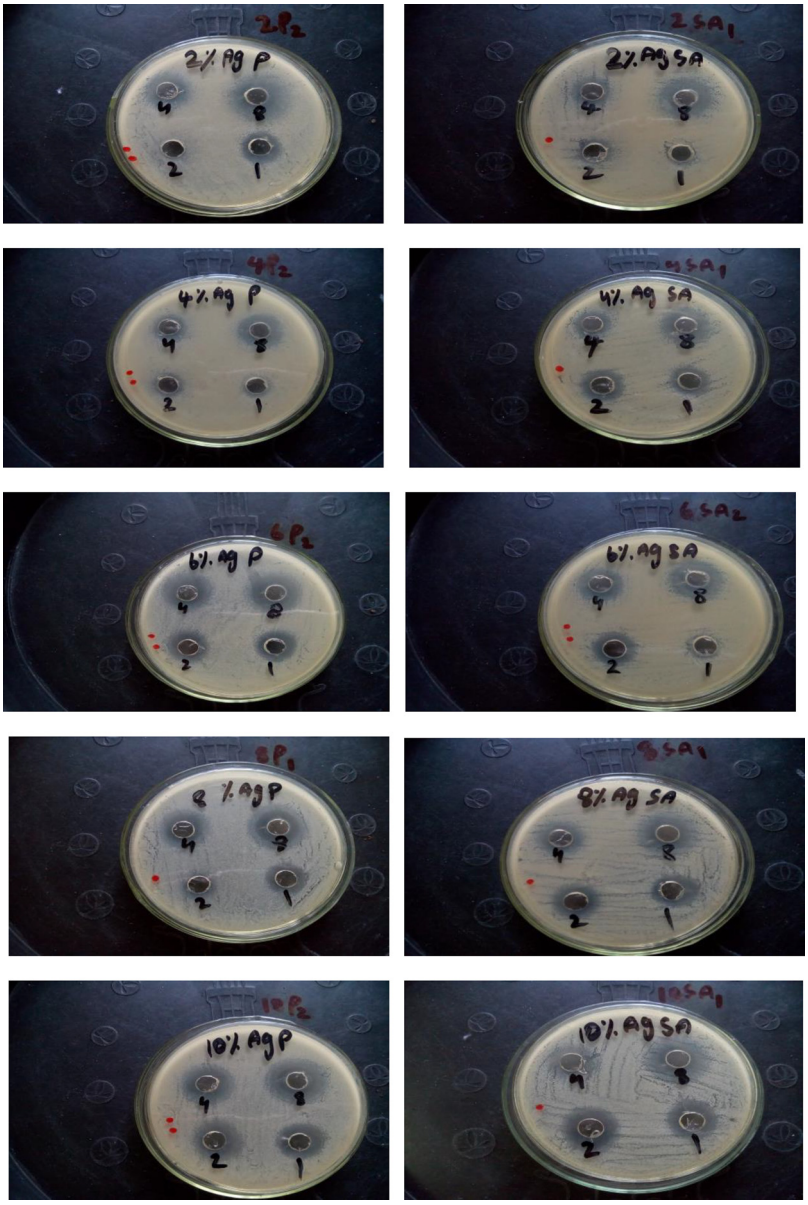

Fig. 5. Antibacterial activity of Ag doped ZnO thin films for 2–10 at. wt. % Ag dopant against *P. aeruginosa and S. aureus.*

3.6. Bacterial cultures and evaluation of antibacterial activities

Staphylococcus aureus (SA), a Gram positive *and Pseudomonas aeruginosa (PA)*, a Gram negative bacteria, were chosen to perform antibacterial experiments. Researchers have used these bacteria for Ag doped ZnO nanoparticles but for the first time in this project antibacterial activity was studied against *Staphylococcus aureus (S. aureus*) and *Pseudomonas aeruginosa (P. aeruginosa)* bacterial strains by varying Ag concentrations in Ag doped ZnO thin films. These strains are not used before for any antibacterial activity of Ag doped ZnO thin films. So far *Escherichia Coli* (*E. Coli*) was used by researchers Thongsuriwong et al. [37] to study the antibacterial activity of Ag doped ZnO thin films. Sterilization in an autoclave was done prior to the experiments. Nutrient agar was used as source for culturing *S. aureus* and *P. aeruginosa* at 37 °C in an incubator. The antibacterial activity of Ag-doped ZnO was measured by agar well diffusion method. Detailed procedure of agar well diffusion method is reported by Kayani et al. [51].

The petri plates utilized in the investigation were prepared using nutrient agar medium. The bacteria were spread uniformly on the plates making use of sterile cotton swabs. The bacterial inoculum was allowed to stay for 5–10 min and then 4 wells of equal diameter (9 mm) were made in each petri plate with the help of a sterilized cork borer. Finally test solutions of Ag-doped ZnO of various concentrations (2, 4, 6, 8, and 10 mg/mL) were added in repective wells. The zones of inhibition were measured after 24 h incubation.The existence of an inhibition zone in Fig. 5 certainly shows that the procedure of the biocidal activity of Ag doped ZnO includes rupturing of the membrane wall. The oxygen species emitted surface of Ag doped ZnO is the cause of the decay of bacteria. Table 3 the size of the inhibition zone enhanced with a decrease in crystallite size of the Ag doped ZnO (Tables 1a and 1b) owing to the substantial surface area to volume ratio. It is observed that, Ag-doped ZnO nano particles are very affective and the growth of bacteria is significantly inhibited with the increase in concentrations of Ag-doped ZnO nano particles. It is illustrated from the Table 3 that the silver at low concentration (2%) is equally effective as the high concentration of silver (10%). So it is economical to use Ag as antibacterial agent. As *S. aureus* is gram positive and *P. aeruginosa* is gram negative becteria and from the Table 3 it is noticed that *P. aeruginosa and S. aureus* both are vulnerable and have high zone of inhibition at 10% Ag for 8 mg/ml which is 27.5 mm. The minimum inhibition zone of 13 mm

Table 3
Antibacterial Activity Ag doped ZnO and control.

Dilution Conc	2% Ag		4% Ag		6% Ag		8% Ag		10% Ag		Control	
	P.A	S.A	P.A	S.A	P.A	S.A	P.A	S.A	P.A	S.A	P.A	S.A
1	15.5 ± 2.12	13 ± 1.41	13.5 ± 0.70	16 ± 1.41	17.5 ± 2.12	14 ± 0	15 ± 2.82	18.5 ± 2.12	18 ± 5.65	16.5 ± 3.53	10.5 ± 0.70	11 ± 1.41
2	12 ± 2.82	14.5 ± 0.70	16 ± 1.41	17.5 ± 2.12	19.5 ± 0.70	16.5 ± 2.12	15.5 ± 0.70	19 ± 0	20.5 ± 2.12	19 ± 1.41	11 ± 1.41	13.5 ± 2.12
4	19 ± 1.41	18.5 ± 0.70	18 ± 1.41	20.5 ± 2.12	22.5 ± 0.70	19.5 ± 0.70	19.5 ± 2.12	21 ± 1.41	22.5 ± 0.70	22.5 ± 2.12	15.5 ± 2.12	14.5 ± 0.70
8	26 ± 0	25 ± 1.41	20.5 ± 0.70	23.5 ± 0.70	24 ± 0	23.5 ± 0.70	25 ± 0	24.5 ± 0.70	26.5 ± 3.53	26.5 ± 0.70	19.5 ± 0.70	19.5 ± 0.70

for *P. aeruginosa* was observed at 2% Ag for 2 mg/ml concentration and for *S. aureus* the low inhibition zone of 14 mm was at 2% Ag for 1 mg/ml concentration. These inhibition zones are larger than earlier reported results [52,53]. Silver doping in ZnO is probed by many researchers and have enhanced antibacterial activity than ZnO against many bacterial strains [54,55].

The release of extremely reactive species OH^-, H_2O_2 and O_2^{2-} can be elaborated by following reactions.

$ZnO + hv \rightarrow h^+ + e^-$

$h^+ + H_2O \rightarrow OH^- + H^+ ; e^- + O_2 \rightarrow O_2^-$

$O_2^- + H^+ \rightarrow HO_2$

$H^+ + HO_2 + e^- \rightarrow H_2O_2$

$H_2O_2 + O_2^- \rightarrow OH^- + O_2 + OH^-$

The emission of H_2O_2 relies on the surface area of Ag doped ZnO, which results in more oxygen species on the surface and the enhanced antibacterial activity for the tiny nano-particles. Less the size of crystallites, more crystallites are used to cover a bacterial colony which liberates large active oxygen species to be used to crush bacteria completely.

Being negatively charged, the hydroxyl radicals (OH^-) and superoxides (O_2^-) can not get inside the cell membrane and stay on the surface of the bacteria; while, O_2 and H_2O_2 can enter into the cell. As Ag doped ZnO destroys the cell membrane, they stay on the dead bacteria and emit peroxides hence displaying high bactericidal efficacy. Ag doped ZnO nano-particles are harmless and generally used as antimicrobial agent, but they may be dangerous owing to their small size and uncertain properties [52]. Deposited synthesized Ag-doped ZnO might act as replacement of conventional antibiotics and can be used in medicine and pharmaceutics as sterile coatings and wound dressings. The discoveries in this research can be used in medical gadgets that are coated with nano-particles against bacteria and virus.

4. Conclusions

Ag doped ZnO thin films were successfully dip coated on glass substrates by varying Ag dopant percentage between 2–10 wt.%. The role of Ag to tailor the properties of ZnO thin films were studied. Ag doped deposited ZnO films are poly-crystalline in nature with wurtzite hexagonal structure. It was noted that optical transmission was decreased with an increase in Ag dopant percentage. The band gap of thin films has a decreasing trend with an increase in Ag dopant percentage. Ag doped ZnO caused greater damage to the cell membrane of *P. aeruginosa and S. aureus* bacteria and the antibacterial effect are equally effective at the low Ag concentration of 2 at. wt. %. as the high concentration of 10 at. wt. %.

References

[1] L. Schmidt-Mende, J.L. MacManus-Driscoll, ZnO–nanostructures, defects, and devices, Mater. Today 10 (2007) 40–48.

[2] F.J. Ramos, M.C. Lopez-Santos, E. Guill, M.K. Nazeerudding, M. Gratzel, A.R. Gonzalez-Elipe, S. Ahmad, Perovskite solar cells based on nanocolumnar plasma-deposited ZnO thin films, Chem. Phys. Chem. 15 (6) (2014) 1148–1153.

[3] A. Wei, L. Pan, W. Huang, Recent progress in the ZnO nanostructure-based sensors, Mater. Sci. Eng. B 176 (18) (2011) 1409–1421.

[4] C.X. Xu, C. Yang, B.X. Gu, S.J. Fang, Nanostructured ZnO for biosensing applications, Chin. Sci. Bull. 58 (21) (2013) 2563–2566.

[5] J.Y. Kim, S.Y. Jo, G.J. Sun, A. Katoch, S.W. Choi, S.S. Kim, Tailoring the surface area of ZnO nanorods for improved performance in glucose sensors, Sens. Actuators B Chem. 192 (2014) 216–220.

[6] I. Perelshtein, G. Applerot, N. Perkas, E. Wehrschetz-Sigl, A. Hasmann, G.M. Guebitz, A. Gedanken, Antibacterial properties of an in situ generated and simultaneously deposited nanocrystalline ZnO on fabrics, ACS Appl. Mater. Interfaces 1 (2009) 361–366.

[7] B. Li, Y. Wang, Facile synthesis and enhanced photocatalytic performance of flower-like ZnO hierarchical microstructures, J. Phys. Chem. C 114 (2010) 890–896.

[8] Y. Xiang, X. Liu, C. Mao, X. Liu, Cui Z, X. Yang, K.W.K. Yeung, Y. Zheng, S. Wu, Infection-prevention on Ti implants by controlled drug release from folic acid/ZnO quantum dots sealed titania nanotubes, Mater. Sci. Eng.: C 85 (2018) 214–224.

[9] Y. Li, X. Liu, L. Tan, Z. Cui, X. Yang, K.W.K. Yeung, H. Pan, S. Wu, Construction of N-halamine labeled silica/zinc oxide hybrid nanoparticles for enhancing

antibacterial ability of Ti implants, Mater. Sci. Eng. C 76 (2017) 50–58.
[10] Y. Zhu, X. Liu, K.W.K. Yeung, P.K. Chu, S. Wu, Biofunctionalization of carbon nanotubes/chitosan hybrids on Ti implants by atom layer deposited ZnO nanostructures, Appl. Surf. Sci. 400 (2017) 14–23.
[11] Z.N. Kayani, I. Shah, B. Zulfiqar, S. Riaz, S. Naseem, A. Sabah, Structural, optical and magnetic properties of nano-crystalline Co doped ZnO thin films grown by sol–gel, Zeitschrift für Naturforschung A 73 (1) (2018) 13–21.
[12] Z.N. Kayani, M. Siddiq, S. Riaz, S. Naseem, Optical, magnetic and structural properties of Cr-doped ZnO thin films by sol–gel dip coating method, Mater. Res. Express 4 (9) (2017) 096403.
[13] Z.N. Kayani, S.S. Naqvi, S. Riaz, S. Naseem, S. Iram, Influence of annealing temperature on the structural, optical and magnetic properties of two-phase MnZnOx(x = 1, 3) thin films grown by a sol–gel method, J. Aust. Cer. Soc. 53 (2) (2017) 864–873.
[14] F. Khan, S.-H. Baek, J.H. Kim, Enhanced charge transport properties of Ag and Al co-doped ZnO nanostructures via solution process, J. Alloys Compd. 682 (2016) 232–237.
[15] Y. Al-Hadeethia, A. Umarc, A.A. Ibrahim, S.H. Al-Henitia, R. Kumarf, S. Baskoutase, B.M. Raffah, Synthesis, characterization and acetone gas sensing applications of Ag doped ZnO nano-needles, Ceram. Int. 43 (2017) 6765–6770.
[16] Y. Yan, M. Al-Jassim, S.-H. Wei, Doping of ZnO by group-Ib elements, Appl. Phys. Lett. 89 (18) (2006) 181912.
[17] X. Xie, C. Mao, X. Liu, Y. Zhang, Z. Cui, X. Yang, K.W.K. Yeung, H. Pan, P.K. Chu, S. Wu, Synergistic bacteria Killing through photodynamic and physical actions of graphene oxide/Ag/collagen coating, ACS Appl. Mater. Interfaces 9 (2017) 26417–26428.
[18] X. Xie, C. Mao, X. Liu, L. Tan, Z. Cui, X. Yang, S. Zhu, Z. Li, X. Yuan, Y. Zheng, K.W.K. Yeung, P.K. Chu, S. Wu, Tuning the bandgap of photo-sensitive polydopamine/Ag_3PO_4/graphene oxide coating for rapid, noninvasive disinfection of implants, ACS Cent. Sci. 4 (2018) 724–738.
[19] C. Mao, Y. Xiang, X. Liu, Z. Cui, X. Yang, K.W.K. Yeung, H. Pan, X. Wang, P.K. Chu, S. Wu, Photo-inspired antibacterial activity and wound healing acceleration by hydrogel embedded with Ag/Ag@AgCl/ZnO nanostructures, ACS Nano 11 (9) (2017) 9010–9021.
[20] F. Xian, K. Miao, X. Bai, Y. Ji, F. Chen, X. Li, Characteraction of Ag-doped ZnO thin film synthesized by sol–gel method and its using in thin film solar cells, Optik 124 (2013) 4876–4879.
[21] N.L. Tarwal, P.S. Patil, Enhanced photoelectrochemical performance of Ag–ZnO thin films synthesized by spray pyrolysis technique, Electrochim. Acta 56 (2011) 6510–6516.
[22] N. Padmavathy, R. Vijayaraghavan, Enhanced bioactivity of ZnO nanoparticles—an antimicrobial study, Sci. Technol. Adv. Mater. 9 (2008) 035004.
[23] F. Elmi, H. Alinezhad, Z. Moulana, F. Salehian, S.T. Mohseni, F. Asgharpour, H. Fallah, M.M. Elmi, The use of antibacterial activity of ZnO nanoparticles in the treatment of municipal wastewater, Water Sci. Technol. 70 (5) (2014) 763–770.
[24] J.S. Kim, E. Kuk, K.N. Yu, J.H. Kim, S.J. Park, H.J. Lee, S.H. Kim, Y.K. Park, Y.H. Park, C.Y. Hwang, Y.K. Kim, Y.S. Lee, D.H. Jeong, M.H. Cho, Antimicrobial effects of silver nanoparticles, Nanomed.: Nanotechnol. Biol. Med. 3 (2007) 95–101.
[25] Y. Xiang, J. Li, X. Liu, Z. Cui, X. Yang, K.W.K. Yeung, H. Pan, S. Wu, Construction of poly(lactic-co-glycolic acid)/ZnO nanorods/Ag nanoparticles hybrid coating on Ti implants for enhanced antibacterial activity and biocompatibility, Mater. Sci. Eng. C 79 (2017) 629–637.
[26] Y. Zhang, X. Liu, Z. Li, S. Zhu, X. Yuan, Z. Cui, X. Yang, P.K. Chu, S. Wu, Nano Ag/ZnO-incorporated hydroxyapatite composite coatings: highly effective infection prevention and excellent osteointegration, ACS Appl. Mater. Interfaces 10 (2018) 1266–1277.
[27] S.K. Singh, R. Singhal, V.V. Siva Kumar, Study on swift heavy ions induced modifications of Ag-ZnO nanocomposite thin film, Superlatt. Microstruct. 103 (2017) 195–204.
[28] H. Sutanto, S. Wibowo, I. Nurhasanah, E. Hidayanto, Optical and microstructure of thin film of Ag-doped ZnO synthesized by sol–gel, AIP Conf. Pro. 1755 (2016) 150001–150004.
[29] S.M. Ali, W.A. Farooq, M.R. Baig, M.A. Shar, M. Atif, S.S. Alghamdi, M.S. Algarawi, N. UR-Rehman, M.H. Aziz, Structural and optical properties of pure and Ag doped ZnO thin films obtained by sol–gel spin coating technique, Mater. Sci. 33 (3) (2015) 601–605.
[30] N.Y. Jamil, S.A. Najim, A.M. Muhammed, V.M. Rogoz, Preparation, structural and optical characterization of ZnO/Ag thin film by CVD, Proc. Int. Con. Nanomater.: Appl. Pro. 3 (2) (2014) 02NEA09 (1–3).
[31] P. Amornpitoksuk, S. Suwanboon, S. Sangkanu, A. Sukhoom, J. Wudtipan, K. Srijan, S. Kaewtaro, Synthesis, photocatalytic and antibacterial activities of ZnO particles modified by diblock copolymer, Powder Technol. 212 (3) (2011) 432–438.
[32] S.S. Alias, A.B. Ismail, A.A. Mohamad, Effect of pH on ZnO nanoparticle properties synthesized by sol–gel centrifugation, J. Alloys 499 (2010) 231–237.
[33] H. Noei, H. Qiu, Y. Wang, E. Löffler, C. Wöll, M. Muhler, The identification of hydroxyl groups on ZnO nanoparticles by infrared spectroscopy, Phys. Chem. Chem. Phys. 10 (2008) 7092–7097.
[34] B.D. Ahn, H.S. Kang, J.H. Kim, G.H. Kim, H.W. Chang, S.Y. Lee, Synthesis and analysis of Ag-doped ZnO, J. Appl. Phys. 100 (2006) 093701.
[35] M.F. Khan, A.H. Ansari, M. Hameedullah, E. Ahmad, F.M. Husain, Q. Zia, U. Baig, M.R. Zaheer, M.M. Alam, A.M. Khan, Z.A. AlOthman, I. Ahmad, G.M. Ashraf, G. Aliev, Sci. Rep. 6 (2016) 1–12.
[36] C. Karunakaran, V. Rajeswari, P. Gomathisankar, Combustion synthesis of ZnO and Ag-doped ZnOand their bactericidal and photocatalytic activities, Superlatt. Microstruct. 50 (2011) 234–241.
[37] K. Thongsuriwong, P. Amornpitoksuk, S. Suwanboon, Photocatalytic and antibacterial activities of Ag-doped ZnO thin films prepared by a sol–gel dip-coating method, J. Sol–Gel Sci. Technol. 62 (2012) 304–312.
[38] P. Scherrer, Nachrichten von der Gesellschaft der Wissenschaften zu Göttingen, Mathematisch-Physikalische Klasse 2 (1918) 98–100.
[39] S.C. Barret, B.T. Massalski, Structure of Metals, Pergamon Press, Oxford, 1980.
[40] M. Dehimi, T. Touam, A. Chelouche, F. Boudjouan, D. Djouadi, J. Solard, A. Fischer, A. Boudrioua, A. Doghmane, Effects of low Ag doping on physical and optical waveguide properties of highly oriented sol–gel ZnO thin films, Adv. Cond. Matter Phys. 2015 (2015) 1–10.
[41] G.A. Nilens, Deep Imparity in Semiconductors, Wiley –Inter-science publication, 1973.
[42] Ü. €Ozgür, Y.I. Alivov, C. Liu, A. Teke, M.A. Reshchikov, S. Dogan, V. Avrutin, S.J. Cho, H. Morkoçd, A comprehensive review of ZnO materials and devices, J. Appl. Phys. 98 (2005) 041301.
[43] S.M. Hosseini, I.A. Sarsari, P. Kameli, H. Salamati, Effect of Ag doping on structural, optical, and photocatalytic properties of ZnO nanoparticles, J. Alloys Compd. 640 (2015) 408–415.
[44] M.K. Gupta, N. Sinha, B. Kumar, p-Type k-doped ZnO nanorods for optoelectronic applications, J. Appl. Phys. 109 (8) (2011) 083532.
[45] J. Sing, "Optical Properties of Condensed Matter and Applications", Wiley Series in Materials for Electronic & Optoelectronic Applications, Jonn Wiley & Sons Ltd, England, 2006.
[46] L.K. Chopra, Thin Film Devices Application, Plenum Press, New York, 1983.
[47] L. Eckortova, Physics of Thin Films, plenum press, 1977.
[48] J.F. Eloy, Power Lasers, National Sch. Phys. John Wiley and Sons, Grenoble, France, 1984, p. 59.
[49] J.I. Pankove, Optical Processes in Semiconductors 91 Dover Publications, Inc., New York, 1975.
[50] J. Tauc, Amorphous and Liquid Semiconductors, Plenum Press, New York, 1974.
[51] Z.N. Kayani, A. Kamran, Z. Saddiqe, S. Riaz, S. Naseem, Probe of ZrTiO2 thin films with TiO2-ZrO2 binary oxides deposited by dip coating technique, J. Photochem. Photobiol. B: Biol. 183 (2018) 357–366.
[52] S. Shahid, S.A. Khan, W. Ahmad, U. Fatima And, S. Knawal, Size-dependent bacterial growth inhibition and antibacterial activity of Ag-doped ZnO nanoparticles under different atmospheric conditions, ind, J. Pharm. Sci. 80 (1) (2018) 173–180.
[53] F.H. Dowlatababdi, G. Amiri, M.M. Sichani, Investigation of the antimicrobial effect of silver doped zinc oxide nanoparticles, Nanomed. J. 4 (1) (2017) 50–54.
[54] R. Vinothini, D. Bavya, Effect of Ag doping on structural, optical and antibacterial behavior ZnO nanoparticles, Int. J. Eng. Sci. Adv. Comput. Bio-Technol. 7 (7) (2017) 14247–142501.
[55] V. Kumara, J. Prakashb, J.P. Singhd, K.H. Chaed, C. Swarte, O.M. Ntwaeaborwaf, H.C. Swartb, V. Duttaa, Role of silver doping on the defects related photoluminescence and antibacterial behaviour of zinc oxide nanoparticles, Colloids Surf. B Biointerfaces 159 (2017) 191–199.